Chinese Chemical Letters 36 (2025) 110153

Contents lists available at ScienceDirect

Chinese Chemical Letters

journal homepage: www.elsevier.com/locate/cclet

Cascading oxidoreductases-like nanozymes for high selective and sensitive fluorescent detection of ascorbic acid

Ying Wang[1], Hong Yang[1], Caixia Zhu[1], Qing Hong, Xuwen Cao, Kaiyuan Wang, Yuan Xu, Yanfei Shen*, Songqin Liu, Yuanjian Zhang*

Jiangsu Engineering Laboratory of Smart Carbon-Rich Materials and Devices, Jiangsu Province Hi-Tech Key Laboratory for Bio-Medical Research, School of Chemistry and Chemical Engineering, Medical School, Southeast University, Nanjing 211189, China

ARTICLE INFO

Article history:
Received 4 March 2024
Revised 20 June 2024
Accepted 20 June 2024
Available online 22 June 2024

Keywords:
Nanozyme
Fluorescence
Selectivity
Sensitivity
Ascorbic acid

ABSTRACT

Compared with natural enzymes, nanozymes have the advantages of high stability and low cost; however, selectivity and sensitivity are key issues that prevent their further development. In this study, we report a cascade nanozymatic system with significantly improved selectivity and sensitivity that combines more substrate-specific reactions and sensitive fluorescence detection. Taking detection of ascorbic acid (AA) as an example, a cascade catalytic reaction system consisting of oxidase-like N-doped carbon nanocages (NC) and peroxidase-like copper oxide (CuO) improved the reaction selectivity in transforming the substrate into the target product by more than 1200 times against the interference of uric acid. The cascade catalytic reaction system was also applicable for transfer from open reactors into a spatially confined microfluidic device, increasing the slope of the calibration curves by approximately 1000-fold with a linear detection range of 2.5 nmol/L to 100 nmol/L and a low limit of detection of 0.77 nmol/L. This work offers a new strategy that achieves significant improvements in selectivity and sensitivity.

Owing to advantages such as high stability, low cost, good biocompatibility, and long-term storage, nanozymes have been widely used in the field of biosensing [1–6]. Nevertheless, they face formidable challenges in the development of sensing systems with high selectivity without biorecognition units [7]. Numerous methods have been explored for increasing the sensing selectivity of nanozymes [8]. For instance, simulating natural enzyme active sites by structural engineering [9], molecular self-assembly [10], and molecular imprinting [11] has intrinsically improved the substrate selectivity of nanozymatic reactions. Inspired by the operation principle of metabolism processes in living, our group reported cascading nanozymes could significantly improve biosensing selectivity in an extrinsic manner [12]. Beyond the mainstream structural efforts, the substrate channeling and screening can be mimicked as a simple but highly efficient approach to address the constraints of nanozymes for highly selective biosensing. Along this line, the sensing selectivity of nanozymes can be further improved by increasing the number of cascade reactions [13,14], improving the substrate specificity of each cascade reaction [15], and/or using a more sensitive output signal [16]. Notably, despite the success of these strategies, studies on improving the selectivity of nanozymes are still in their infancy.

Ascorbic acid (AA) is a water-soluble vitamin necessary for regulating body metabolism and maintaining normal physiological functions [17,18]. It promotes the synthesis of collagen and neurotransmitters, and maintains healthy skin and normal function of the nervous system as well [19]. An imbalance in the level of AA may lead to tissue damage and related diseases [20]. Therefore, it is of great significance to develop highly selective and sensitive methods for AA detection. A variety of analytical techniques are available for the detection of AA, such as electrochemical methods [21], liquid chromatograph [22], chemiluminescence [23], and spectrophotometry [24–26]. Despite their wide applications, these technologies require significant advancements in terms of sensitivity and selectivity.

Herein, we report a highly sensitive and selective fluorescent bioassay of AA using cascading N-doped carbon nanocages (NC) and copper oxide (CuO). Due to the second nanozyme in the cascade reaction, CuO, catalyzed hydrogen peroxide to produce hydroxyl radicals, which reacted more specifically with terephthalic acid (TA) to produce fluorescent signals. As a result, the relative reactivity of AA to uric acid (UA) was as high as 1242-fold. Density functional theory (DFT) revealed the mechanism of the CuO-

* Corresponding authors.
E-mail addresses: Yanfei.Shen@seu.edu.cn (Y. Shen), Yuanjian.Zhang@seu.edu.cn (Y. Zhang).
[1] These authors contributed equally to this work.

https://doi.org/10.1016/j.cclet.2024.110153
1001-8417/

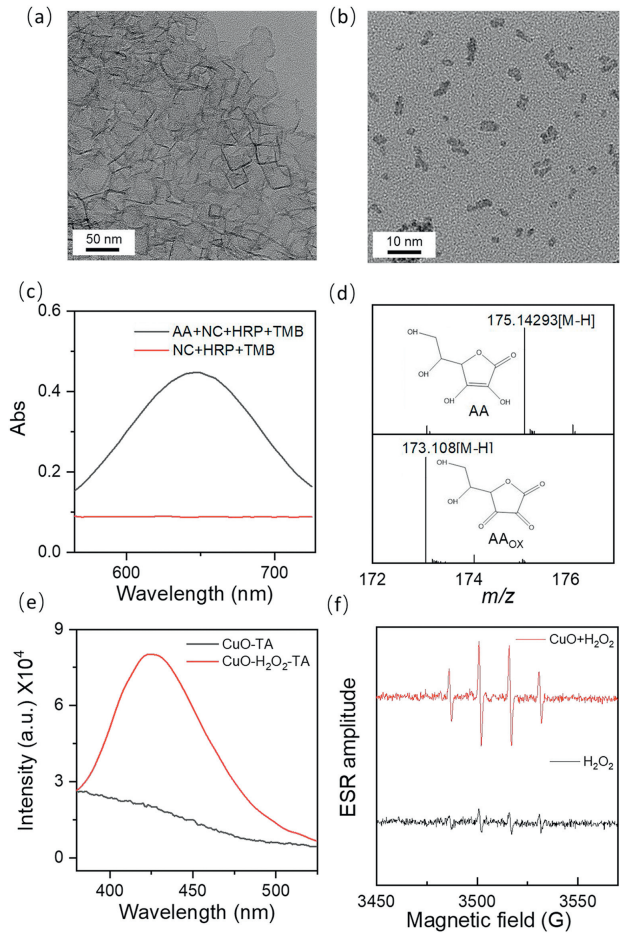

Fig. 1. TEM images of (a) NC and (b) CuO. (c) UV–vis spectra of the TMB-HRP kit for the NC-catalyzed reaction before and after adding AA. (d) ESI-MS spectra of AA before and after the catalytic oxidation by NC. (e) Fluorescence spectra of TA before and after oxidation with H_2O_2. (f) ESR spectra of H_2O_2 before and after addition of CuO.

catalyzed chromogenicity of terephthalic acid (TA), further suggesting better substrate specificity for this reaction. The proposed NC–CuO cascade system was used for AA detection by combining microfluidic technology. Because of the more sensitive fluorescence signal output, the sensor exhibits a linear concentration range of AA from 2.5 nmol/L to100 nmol/L with a limit of detection (LOD) of 0.77 nmol/L (S/N = 3).

The NC was prepared by the MgO template method using pyridine as a precursor at approximately 800 °C [27]. Scanning electron microscopy (SEM) images showed that NC is a cubic hollow nanocage structure (Fig. S1 in Supporting information). The transmission electron microscopy (TEM) images in Fig. 1a further disclosed these nanocages interconnected to form micrometer-sized nanosheets, which further assembled into 3D flower-like particles with a large intersheet space. X-ray photoelectron spectroscopy (XPS) also confirmed the successful synthesis of NC. As shown in Fig. S2 (Supporting information), the N 1s XPS spectra were deconvoluted into four peaks at 397.8, 399.2, 400.6, and 401.8 eV, corresponding to pyridinic N, pyrrolic N, graphitic N, and oxidized N, respectively. Thus, the hierarchical structure along with dopants endowed NC with a large specific surface area, which would facilitate rapid charge (ion and electron) transfer and promote the efficiency of nanozymatic reactions [28].

CuO was fabricated using a rapid precipitation method [29]. Fig. 1b shows that the average particle diameter of CuO was approximately 6.0 nm. X-ray diffraction (XRD) was used to determine the crystal structure of CuO (Fig. S3 in Supporting information). The main diffraction peaks of CuO were observed at 2θ degrees of 32.6 (110), 35.6 ($\bar{1}11$), 38.7 (111), 48.8 ($\bar{2}02$), which is consistent with CuO [30]. The high-resolution X-ray photoelectron spectra (XPS) in Fig. S4 (Supporting information) provided additional bonding information. The Cu 2p XPS spectra exhibited two main peaks at 933.08 eV (Cu $2p_{3/2}$) and 953.18 eV (Cu $2p_{1/2}$), demonstrating pure copper(II) oxide [31]. Moreover, different morphologies of CuO were also synthesized to explore the structure-function relationship. It was found that the morphologies of CuO had a negligible influence on the catalytic oxidation activity (Fig. S5 in Supporting information). These results confirmed the successful synthesis of the CuO NPs.

The oxidase-like activity of NC was explored using UV–vis spectroscopy. As shown in Fig. S6 (Supporting information), the typical absorption of AA at 265 nm disappeared after incubation with NC in PBS. To validate the product of the catalytic oxidation of AA by NC, a standard 3,3′,5,5′-tetramethylbenzidine-Horseradish peroxidase (TMB-HRP) kit was employed. After the addition of AA to the reaction solution, a typical characteristic peak of TMB_{ox} was observed at 652 nm, whereas negligible absorbance was obtained in the control reaction system without AA (Fig. 1c). This demonstrates that H_2O_2 was produced during the oxidation of AA catalyzed by NC. Subsequently, the oxidized products were verified by electrospray mass spectrometry (ESI-MS). Before oxidation, an AA fragment ([M-H]) was observed at 175.14 (Fig. 1d). Notably, a dehydrogenated oxidation product of AA (173.11) was observed after the addition of AA to the NC catalytic reaction system, which further demonstrated the oxidase-like properties of NC. To quantitatively evaluate the catalytic activity, a steady-state kinetic experiment was performed by varying the concentration of AA. Briefly, the enzymatic kinetic constants, including the Michaelis–Menten constant (K_m) and maximum reaction velocity (V_{max}) of the NC nanozymes, were obtained by steady-state kinetic assays (Fig. S7 in Supporting information). The K_m and V_{max} values of NC were *ca.* 15.97 μmol/L and 5.23×10^{-6} mol L^{-1} s^{-1}, indicative of good affinity and catalytic activity for substrates.

In this study, TA was used as a substrate to investigate the peroxidase-like activity of CuO [32]. The POD-like catalytic activity of CuO was confirmed by comparative experiments. As shown in Fig. 1e, the addition of H_2O_2 significantly increased the fluorescence intensity (red line) compared with that of the CuO-TA system without H_2O_2 (black line). To understand the catalytic mechanisms of CuO in peroxidase-like activity, the intermediate reactive species were studied using scavenger trapping experiments. As illustrated in Fig. S8 (Supporting information), the catalytic activity was significantly reduced when isopropanol was added to the system, indicating that H_2O_2 generated hydroxyl radicals (•OH) as a major step. Electron spin resonance (ESR) spectra also supported this speculation. As shown in Fig. 1f, the characteristic peaks of DMPO-•OH adducts with a signal intensity of 1:2:2:1 were observed during the peroxidase-like reaction by CuO. Steady-state kinetics were used to quantitatively characterize the peroxidase-like activity of CuO. As shown in Fig. S9 (Supporting information), typical Michaelis–Menten curves were obtained, showing a V_{max} of 1.9919×10^{-7} mol L^{-1} s^{-1} and K_m of 72.98 mmol/L. Thus, CuO exhibited high POD-like catalytic activity in the oxidation of TA with H_2O_2, and the product could be sensitively detected by fluorescence.

Density functional theory (DFT) calculations were performed to gain further insight into the mechanisms underlying of H_2O_2 to produce •OH catalyzed by CuO. For this purpose, both the adsorption process of H_2O_2 and the process of catalyzing the transition state of H_2O_2 were calculated. For simplicity, the most studied and observed CuO (111) facet (Fig. S10a in Supporting information) was chosen as the adsorption substrate. When a H_2O_2 molecule was

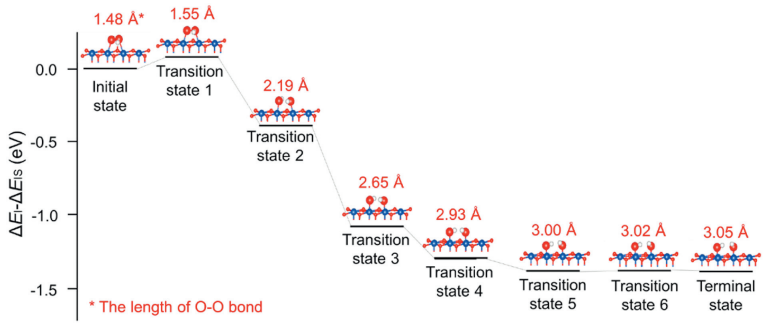

Fig. 2. Scheme of the reaction pathway for H_2O_2 activation on the CuO surface. Oxygen atoms: red; hydrogen atoms: white; Cu atoms: blue. For clarity, the sizes of the O and H atoms in H_2O_2 are not in scale.

supposed to be adsorbed by the Cu site on the CuO (111) surface, the system energy was reduced by 0.53 eV (Fig. S10b in Supporting information). Under the attraction of two Cu sites, the O–O bond of H_2O_2 continuously elongated, ultimately breaking to form two ·OH radicals (Fig. 2). During the reaction, when the O–O bond was stretched, the system needs to cross a small energy barrier of 0.09 eV. After stable adsorption of two ·OH radicals, an energy of up to 1.39 eV ($E_{TS} - E_{IS}$) was released. DFT calculations demonstrated that the CuO-catalyzed ·OH production from H_2O_2 conformed to the thermodynamic law, which was consistent with the experimental results (Fig. 1f) and provided a theoretical foundation for improving the selectivity of TA molecule oxidation.

Owing to its advantages of high detection sensitivity and fast reaction speed, TMB has a wide range of applications in the fields of biochemistry, pharmaceuticals, and the environment [33–36]. However, several deficiencies of TMB are often overlooked. As a typical chromogenic substrate, TMB generally undergoes one-electron oxidation, but the product is unstable, which easily undergoes one more electron oxidation into the yellow product [37]. In addition, because TMB has poor selectivity in oxidants, it can be catalyzed by different reactive oxygen free radicals. Both limitations of TMB significantly compromise the sensing accuracy. As known, fluorescence detection methods are widely used in the field of analytical chemistry due to their high sensitivity and convenient detection [38]. On the other hand, fluorescent probes are often able to specifically bind certain groups or molecules with better substrate specificity, which ensures the selectivity and sensitivity of the reaction [39]. It was experimentally found that TA had better reaction specificity than TMB, which can only be oxidized in the presence of ·OH (Fig. 3a). Therefore, TA was chosen as the chromogenic substrate for the selective and sensitive detection of AA in this study.

When H_2O_2 was added to CuO-TA system, H_2O_2 can be catalyzed to produce ·OH. TA can then be oxidized to form TAOH. Considering that TAOH has both UV and fluorescence responses, UV–vis and fluorescence spectra were employed. As shown in Fig. 3b, the detection limit obtained using the TAOH fluorescence signal was much lower than that obtained using the UV–vis signal. Therefore, considering the sensitivity of fluorescence, we constructed a fluorescence cascade reaction based on the NC–CuO system. A cascaded detection strategy with high sensitivity and selectivity was developed based on the reaction specificity of TA and a sensitive fluorescence detection method.

It is important to construct the cascade system by rationally selecting nanozymes with appropriate activities. To demonstrate the advantages of NC, several other nanozymes with oxidase-like activity such as Pt/C, Fe–N–C–CM6 (CM6) and Fe–N–C–Me (Me) were cascaded with CuO to catalyze AA oxidation (Fig. 3c). The cascade using Pt/C, CM6 and Me with CuO was found to be less effective than the cascade of NC and CuO. In addition, control experiments confirmed that NC had no catalytic effect on TA (Fig. S11 in Supporting information). Different interference substrates (*e.g.*, Cys, GSH, UA, and AA) were used to study the importance of the nanozyme sequence. It was found that the CuO–NC system could react with all these substrates to produce fluorescence signals (Fig. 3d), indicating that the cascade system constructed in this order was not selective for the detection of substrates. Thus, the NC–CuO cascade system was adopted for the fluorescent detection of AA. As shown in Fig. 3e, NC with oxidase-like activity can catalyze oxygen to generate H_2O_2, and the H_2O_2 can be catalyzed by CuO to produce ·OH. ·OH interacts with TA to produce TAOH, which exhibits strong fluorescence. Based on these results, a simple and sensitive fluorescence detection method was established for the detection of AA.

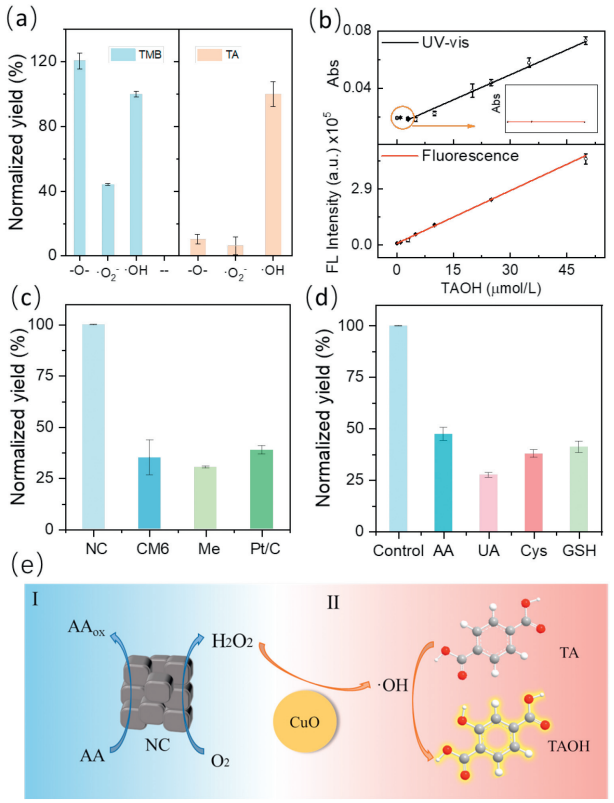

Fig. 3. (a) Reactivity of TMB and TA against various free reactive oxygen radicals. (b) UV–vis and fluorescence spectra of TAOH. (c) Reactivity of the cascade system constructed using different oxidases and CuO. (d) Reactivity of CuO–NC cascade system used to detect different substrates. (e) Scheme of the NC–CuO cascade system.

It should be noted that CuO was chosen for this study for several reasons. First, CuO catalyzes the formation of ·OH from H_2O_2, and the reaction has been demonstrated to have good speci-

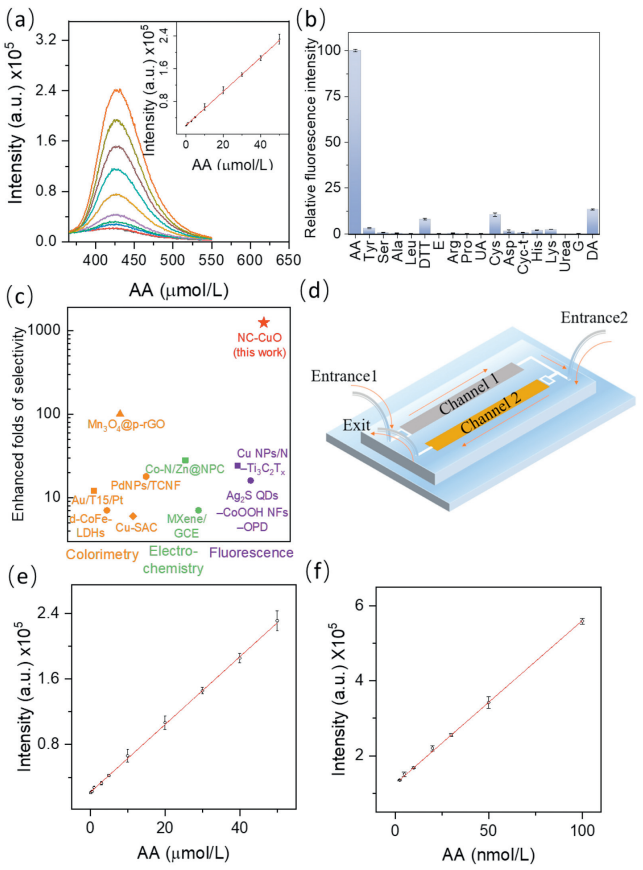

Fig. 4. (a) Fluorescence spectra of TA oxidation products generated from the NC–CuO cascade system with different AA concentrations. Inset: calibration curve of fluorescence intensity with concentration of AA. (b) Fluorescence intensity of the TA oxidation product generated from the NC–CuO nanozyme cascade system using AA and other small molecules as potential interfering substrates. (c) Comparison of the enhanced folds of selectivity for AA using different detection methods [40–48]. (d) Scheme of microfluidic reactor containing cascade NC–CuO. Calibration curves of fluorescence intensity with AA concentration in the (e) open reactor and (f) spatially confined microfluidic reactor.

ficity through experiments and theoretical calculations. Secondly, the $^{\bullet}OH$ produced by CuO catalyzed H_2O_2 can specifically bind to the fluorescent probe TA. In addition, CuO cannot directly catalyze the oxidative color development of TA and does not interfere with the sensing system. All this makes the CuO-catalyzed reaction more specific, enabling the cascade system with better selectivity.

We next explore the sensing AA *via* cascade reaction. Typically, 10 μL of NC suspension was dropped into 1 mL of PBS (0.2 mol/L, pH 6.0) with different AA concentrations. After incubation at 45 °C for 3 min, the NC was removed by filtration. Then, 25 μL of 120 mmol/L TA and 10 μL of 5 mg/mL CuO were added to the supernatants, and the above solution was incubated for 25 min at 45 °C. The fluorescence signal was collected at 423 nm, using an excitation wavelength of 315 nm. Under optimum conditions, the fluorescence intensity increased gradually with an increase in AA concentration, demonstrating that the proposed NC–CuO system can be employed to detect AA. By quantifying the results, calibration curves and the corresponding linear ranges of AA detection were obtained (Fig. 4a). The increase of the fluorescence intensity was proportional to the AA concentration in the range of 0.1–50 μmol/L, with a correlation coefficient of $R^2 = 0.99$. The fitted linear equation was FL intensity = 4140*C* (μmol/L) + 21674. A variety of interferences were introduced into the detection system to assess the selectivity of this fluorescence assay for the detection of AA. Although the concentration of interference was the same as that of AA, a high fluorescence intensity was produced only when AA was present in the system, as shown in Fig. 4b. In particular, without any sophisticated modification of nanozymes and any introduction of natural enzymes, the relative reaction selectivity of AA against UA was up to 1242 fold. The enhanced selectivity for AA based on the nanozymatic system significantly surpassed that of previously reported AA sensors (see Fig. 4c for more details) [40–48]. It showed beyond the mainstream structured efforts, the substrate channeling and screening can be mimicked as a simple but highly efficient approach to address the constraints of nanozymes for high selective biosensing.

Beyond the open reaction system, we further study the sensing of AA with cascade reactions in a microfluidic device. As an emerging technology, microfluidic technology is widely applied in multiple fields, such as materials science and biomedical engineering [49–52]. In microfluidic systems, trace amounts of reactants react at the micrometer scale, and intermediate products are also sealed to minimize competitive cross-reactions to improve reaction efficiency [53–56]. In addition, it can also guide substrates to react with specific cascade sequences [57]. Microfluidic systems provide biological analysis technology advantages such as low cost, high precision, high resolution, and simple operation [58,59]. In this study, as shown in Fig. 4d, the microfluidic device was fabricated by painting NC and CuO on the different channels of polydimethylsiloxane (PDMS). The channel has a length of 40 mm, depth of 0.07 mm, and width of 4 mm. In a microfluidic device, different channels of microfluidic device were loaded with corresponding NC and CuO catalysts, respectively. Polypropylene tubes were used to connect the microfluidic chip and control the flow of the reaction solution. PBS containing different concentrations of AA was pumped into the first reaction channel and allowed to react at 45 °C for 3 min. Subsequently, the reaction solution was pumped into the second reaction channel, while TA was pumped from the downstream inlet. Finally, the reaction solution at the outlet (about 40 μL) was collected in a microcuvette and the signal was detected by fluorescence spectroscopy. As aforementioned, AA would be catalyzed by NC in channel 1, and TA would be later catalytically oxidized by CuO in channel 2 using the produced H_2O_2 from channel 1 as a co-substrate. The final TAOH solution (about 40 μL) from channel 2 was quantitatively analyzed. The increase in the fluorescence intensity was proportional to the AA concentration in the range of 2.5–100 nmol/L with a limit of detection (LOD) of 0.77 nmol/L ($S/N = 3$), which was superior to the open system results and previously reported results (Table 1) [21,24–26,60–63]. Furthermore, as shown in Figs. 4e and f, the slope of the nanozymatic cascade reaction in the microfluidic device improved by approximately 1000-fold compared to the linear slope of the AA assay in the open system. It indicated that the conversion efficiency and associated detection sensitivity were greatly improved. This study provides a strategy for improving sensor selectivity and sensitivity using AA as an example, particularly for trace samples, and is expected to be helpful to other sensing strategies for improving detection selectivity and sensitivity.

To prove the suitability and feasibility of the established platform for AA detection in biological samples, the analytical performance of the sensing strategy was evaluated. Since bovine serum albumin is one of the most widely studied proteins and is similar to human serum albumin, the analytical performance of 10% diluted bovine serum supplemented with AA was evaluated. Recovery rate experiments were performed in the open system. AA was added to the diluted serum samples at concentrations of 5, 25 and 50 μmol/L, and the recoveries of AA mixed with serum samples ranged from 95.1% to 101.6% (Figs. 5a and b). Recovery experiments were also performed in a microfluidic system. AA was added to the diluted serum samples at concentrations of 5, 50 and 100 nmol/L, the recoveries of AA mixed with serum samples ranged from 98.4%

Table 1
Comparison of different methods for AA detection in literature.

Method	Material	Dynamic detection range (μmol/L)	LOD (μmol/L)	Ref.
Fluorescence	CNCs	0.5–100	0.15	[60]
Fluorescence	CuInZnS QDs	0.05–0.25	0.011	[61]
Colorimetry	CuO NP-POM	0.02–500	0.015	[24]
Electrochemistry	$ZnCr_2O_4$	0.01–126	0.01256	[21]
Colorimetry	PtNi/NCFs	1–20	0.94	[26]
Colorimetry	CuNHCNs	1–500	0.0689	[25]
Fluorescence	R-CDs& PDA	0.5–30	0.28	[62]
Fluorescence	LDH-GQDs	5–300	1.73	[63]
Fluorescence	NC–CuO (open reactor)	0.1–50	0.085	This work
Fluorescence	NC–CuO (microfluidic device)	0.0025–0.1	0.00077	This work

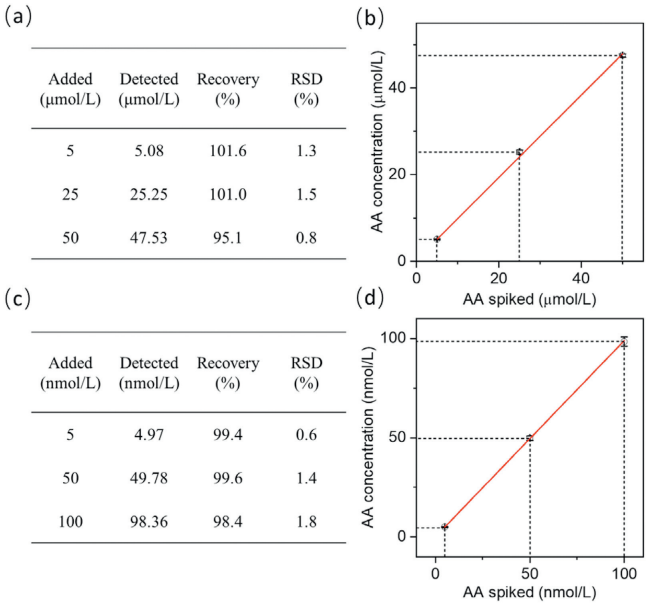

Fig. 5. (a, b) AA recovery assay in an open reactor. (c, d) AA recovery assay of the microfluidic device.

to 99.6% (Figs. 5c and d). These findings confirmed the accuracy and strong dependability of AA detection.

In summary, based on a nanozyme catalytic system with high reaction specificity, we developed a cascaded fluorescence sensing system for the selective and sensitive detection of AA against various interferences. AA was oxidized by NC to produce AA_{ox} and the by-product H_2O_2. The second step of cascade transformation was induced by the addition of CuO nanozymes. Further using the $^{\bullet}OH$ generated by CuO-catalyzed reaction to oxidize TA, a fluorescence sensing platform was constructed for AA with a linear detection range of 2.5-100 nmol/L/0.1-50 μmol/L and a low limit of detection of 0.77 nmol/L/0.085 mol/L in a spatially confined microfluidic reactor and an open reactor, respectively. More importantly, the AA detection by cascaded fluorescence sensing system had excellent selectivity by combining more substrate-specific reaction and stood out from over a dozen interferents, such as UA, urea, Glu without any biorecognition units. Notably, the cascade strategy comprehensively considers the reaction specificity of the nanozymes and the signal output mode. By combining the two, sensing targets with high sensitivity and high selectivity were realized. This study offers a new direction for the design of nanozymatic assays with enhanced sensitivity and selectivity.

Declaration of competing interest

The authors declare that they have no known competing financial interests or personal relationships that could have appeared to influence the work reported in this paper

CRediT authorship contribution statement

Ying Wang: Writing – original draft, Methodology, Investigation. **Hong Yang:** Visualization, Methodology. **Caixia Zhu:** Writing – review & editing, Methodology. **Qing Hong:** Writing – review & editing. **Xuwen Cao:** Methodology. **Yuan Xu:** Methodology. **Yanfei Shen:** Writing – review & editing, Methodology, Funding acquisition. **Songqin Liu:** Writing – review & editing, Methodology. **Yuanjian Zhang:** Writing – review & editing, Supervision, Methodology, Funding acquisition, Conceptualization.

Acknowledgment

This work was supported by the National Natural Science Foundation of China (Nos. 22174014 and 22074015).

Supplementary materials

Supplementary material associated with this article can be found, in the online version, at doi:10.1016/j.cclet.2024.110153.

References

[1] D. Jiang, D. Ni, Z.T. Rosenkrans, et al., Chem. Soc. Rev. 48 (2019) 3683–3704.
[2] C. Peng, R. Pang, J. Li, E. Wang, Adv. Mater. 36 (2023) 2211724.
[3] L. Zhang, H. Wang, X. Qu, Adv. Mater. 36 (2023) 2211147.
[4] S. Ji, B. Jiang, H. Hao, et al., Nat. Catal. 4 (2021) 407–417.
[5] Y. Wang, G. Jia, X. Cui, et al., Chem 7 (2021) 436–449.
[6] D. Chen, Z. Xia, Z. Guo, et al., Nat. Commun. 14 (2023) 7127.
[7] H. Fan, R. Zhang, K. Fan, L. Gao, X. Yan, ACS Nano 18 (2024) 2533–2540.
[8] H. Fan, J. Zheng, J. Xie, et al., Adv. Mater. 36 (2023) 2300387.
[9] B. Yu, W. Wang, W. Sun, C. Jiang, L. Lu, J. Am. Chem. Soc. 143 (2021) 8855–8865.
[10] M. Kim, M. Dygas, Y.I. Sobolev, et al., J. Am. Chem. Soc. 143 (2021) 1807–1815.
[11] Z. Zhang, X. Zhang, B. Liu, J. Liu, J. Am. Chem. Soc. 139 (2017) 5412–5419.
[12] Q. Zhou, H. Yang, X. Chen, et al., Angew. Chem. Int. Ed. 61 (2022) e202112453.
[13] Z. Chen, Y. Yu, Y. Gao, Z. Zhu, ACS Nano 17 (2023) 13062–13080.
[14] F. Rudroff, M.D. Mihovilovic, H. Gröger, et al., Nat. Catal. 1 (2018) 12–22.
[15] W. Gao, J. He, L. Chen, et al., Nat. Commun. 14 (2023) 160.
[16] M. Wamsley, S. Zou, D. Zhang, Anal. Chem. 95 (2023) 17426–17437.
[17] N. Liu, R. Wang, S. Gao, et al., Adv. Mater. 33 (2021) 2105697.
[18] K. Wang, J. Liu, X. Wang, et al., Microchem. J. 172 (2022) 106921.
[19] J. Kim, T. Lee, H.D. Jung, et al., Nat. Commun. 15 (2024) 192.
[20] M. Wang, J. He, S. Li, et al., Nat. Commun. 14 (2023) 1361.
[21] B. Sriram, S. Kogularasu, S.F. Wang, J.K. Sheu, ACS Appl. Nano Mater. 6 (2023) 17593–17602.
[22] H. Iwase, I. Ono, J. Agric. Food Chem. 45 (1997) 4664–4667.
[23] N. Kishikawa, M. El-Maghrabey, Y. Nagamune, et al., Anal. Chem. 92 (2020) 6984–6992.
[24] Y. Xu, P. Li, X. Hu, et al., ACS Appl. Nano Mater. 4 (2021) 8302–8313.
[25] X.S. Tao, Y. Liu, Y. Gan, et al., Analyst 147 (2022) 5419–5427.
[26] Y.W. Mao, J.Q. Li, R. Zhang, A.J. Wang, J.J. Feng, ACS Appl. Nano Mater. 6 (2023) 2805–2812.
[27] S. Chen, J. Bi, Y. Zhao, et al., Adv. Mater. 24 (2012) 5593–5597.
[28] J. Zhao, H. Lai, Z. Lyu, et al., Adv. Mater. 27 (2015) 3541–3545.
[29] J. Zhu, D. Li, H. Chen, et al., Mater. Lett. 58 (2004) 3324–3327.
[30] W. Chen, J. Chen, Y.B. Feng, et al., Analyst 137 (2012) 1706–1712.
[31] S. Sicwetsha, S. Mvango, T. Nyokong, P. Mashazi, J. Nanopart. Res. 23 (2021) 227.
[32] A.L. Hu, Y.H. Liu, H.H. Deng, et al., Biosens. Bioelectron. 61 (2014) 374–378.
[33] X. Zhang, Q. Yang, Y. Lang, X. Jiang, P. Wu, Anal. Chem. 92 (2020) 12400–12406.
[34] Y. Chen, P. Wang, H. Hao, et al., J. Am. Chem. Soc. 143 (2021) 18643–18651.

[35] L. Yu, M. Yu, W. Chen, et al., J. Am. Chem. Soc. 145 (2023) 8375–8388.
[36] B. Li, R. Ma, L. Chen, et al., Nat. Commun. 14 (2023) 6553.
[37] C. Zhu, H. Yang, X. Cao, et al., Anal. Chem. 95 (2023) 16407–16417.
[38] B. Li, J. Qi, F. Liu, et al., Nat. Commun. 14 (2023) 7312.
[39] L. Wu, J. Liu, P. Li, B. Tang, T.D. James, Chem. Soc. Rev. 50 (2021) 702–734.
[40] H. Chen, Z. Cai, J. Gui, et al., J. Mater. Chem. B 11 (2023) 1279–1287.
[41] S.A. Zaidi, H. Sheikh, M. Al-Mahasna, F. Elsin, Int. J. Biol. Macromol. 249 (2023) 126024.
[42] R. Dadigala, R. Bandi, S.Y. Han, G.J. Kwon, S.H. Lee, Int. J. Biol. Macromol. 234 (2023) 123657.
[43] M. Cai, Y. Zhang, Z. Cao, W. Lin, N. Lu, ACS Appl. Mater. Interfaces 15 (2023) 18620–18629.
[44] Y. Ning, Y. Sun, X. Yang, et al., ACS Appl. Mater. Interfaces 15 (2023) 26263–26272.
[45] D. Peng, M. Que, X. Deng, et al., Microchim. Acta 190 (2023) 243.
[46] X. Liu, F. Wu, X. Zheng, et al., ACS Appl. Nano Mater. 6 (2023) 10303–10311.
[47] R. Shanmugam, S. Aniruthan, V. Yamunadevi, et al., Surf. Interfaces 40 (2023) 103103.
[48] J. Huang, C. Shen, H. Gu, et al., ACS Sustain. Chem. Eng. 11 (2023) 17472–17481.
[49] R.G. Rosenthal, X.D. Zhang, K.I. Đurđić, J.J. Collins, D.A. Weitz, Angew. Chem. Int. Ed. 62 (2023) e202303112.
[50] E. Akbari, M. Shahhosseini, A. Robbins, et al., Nat. Commun. 13 (2022) 6800.
[51] A. Das, C. Weise, M. Polack, et al., J. Am. Chem. Soc. 144 (2022) 10353–10360.
[52] A. Méndez-Ardoy, A. Bayón-Fernández, Z. Yu, et al., Angew. Chem. Int. Ed. 59 (2020) 6902–6908.
[53] J. Zhang, J. Chen, S. Peng, et al., Chem. Soc. Rev. 48 (2019) 2566–2595.
[54] K. Ren, Y. Xu, Y. Liu, M. Yang, H. Ju, ACS Nano 12 (2017) 263–271.
[55] Y. Liu, R. Lv, S. Sun, et al., Chin. Chem. Lett. 33 (2022) 807–811.
[56] M.L. Cunha, S.S. da Silva, M.C. Stracke, et al., Anal. Chem. 94 (2021) 41–58.
[57] Q. Liu, H. Wei, Y. Du, TrAC, Trends Anal. Chem. 158 (2023) 116858.
[58] G. Zhang, Y. Wang, W. Zhou, et al., Angew. Chem. Int. Ed. 62 (2023) e202315113.
[59] G.M. Whitesides, Nature 442 (2006) 368–373.
[60] J.H. Zhang, Z.T. Zhang, M.S. Sheng, et al., ACS Appl. Nano Mater. 5 (2022) 5234–5243.
[61] J. Zhang, J. Liu, M. Wang, X. Su, Talanta 214 (2020) 120814.
[62] Q. Xiao, P. Mu, G. Ning, et al., Talanta 264 (2023) 124724.
[63] H. Shi, L. Chen, N. Niu, Sens. Actuators B 345 (2021) 130353.